Journal of Hazardous Materials 431 (2022) 128510

Contents lists available at ScienceDirect

Journal of Hazardous Materials

journal homepage: www.elsevier.com/locate/jhazmat

Research Paper

Vacancy-rich BiO_{2-x} as a highly-efficient persulfate activator under near infrared irradiation for bacterial inactivation and mechanism study

Hongli Sun [a,b], Kemeng Xiao [b,c], Yunfei Ma [a], Shuning Xiao [d], Qitao Zhang [a,*], Chenliang Su [a], Po Keung Wong [b,e,**]

[a] International Collaborative Laboratory of 2D Materials for Optoelectronics Science and Technology of Ministry of Education, Institute of Microscale Optoelectronics, Shenzhen University, Shenzhen 518060, China
[b] School of Life Science, The Chinese University of Hong Kong, Shatin, NT, Hong Kong, China
[c] Center of Super-Diamond and Advanced Films (COSDAF) & Department of Chemistry, City University of Hong Kong, Kowloon Tong, Kowloon, Hong Kong, China
[d] School of Materials Science and Engineering, University of Shanghai for Science and Technology, Shanghai 200093, China
[e] Institute of Environmental Health and Pollution Control, School of Environmental Science and Engineering, Guangdong University of Technology, Guangzhou 510006, China

HIGHLIGHTS

- Persulfate activation was realized under NIR radiation for the first time.
- Vacancy-rich BiO_{2-x} can activate persulfate multiply under NIR radiation.
- Sulfate radical was the key species for NIR-driven bacterial disinfection in 40 min.
- The respiration, ATP synthesis, bacterial membrane and enzymes, etc. were damaged.
- The leakage of DNA and RNA caused the irreversible damage to the bacterial cells.

GRAPHICAL ABSTRACT

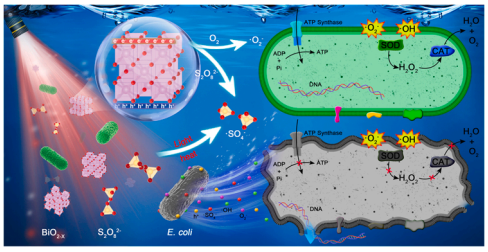

ARTICLE INFO

Editor: Dr. T. Meiping

Keywords:
Vacancy-rich BiO_{2-x}
Persulfate activation
Sulfate radicals
Bacterial inactivation
Near-infrared light irradiation

ABSTRACT

This study, for the first time, developed a novel defective BiO_{2-x} based collaborating system, where the near-infrared light (NIR) irradiation ($\lambda > 700$ nm) initiated persulfate activation and photocatalytic bacterial inactivation simultaneously. Vacancy-rich BiO_{2-x} nanoplates possessed impressive NIR absorption and firstly realized persulfate activation under NIR irradiation. In this collaborating system, on one hand, the persulfate can be transformed into sulfate radicals through light/heat activation mode directly, which would be enhanced by the presence of vacancy-rich BiO_{2-x} owing to its outstanding light and heat absorption ability. On the other hand, the photogenerated electrons can further efficiently react with persulfate and form sufficient reactive sulfate radicals. The sulfate radicals, synergizing with other reactive species (O_2^-, h^+, etc.), achieved a 7-log *Escherichia coli* inactivation within 40 min. The systematic investigation of inactivation mechanism revealed that the reactive species caused the dysfunction of cellular respiration, ATP synthesis and bacterial membrane, followed by the severely oxidative damage to the antioxidative SOD and CAT enzymes and the generation of carbonylated protein. The final leakage of DNA and RNA implied the lethal damage to the bacteria cells. This work provided a

* Corresponding author.
** Corresponding author at: School of Life Science, The Chinese University of Hong Kong, Shatin, NT, Hong Kong, China.
E-mail addresses: qitao-zhang@szu.edu.cn (Q. Zhang), pkwong@cuhk.edu.hk (P.K. Wong).

https://doi.org/10.1016/j.jhazmat.2022.128510
Received 6 December 2021; Received in revised form 27 January 2022; Accepted 15 February 2022
Available online 18 February 2022

new insight into the persulfate associated NIR driven remediation technology of controlling microbial contaminants.

1. Introduction

The waterborne diseases caused by pathogenic microorganisms have posed a great threat to both the developed and developing countries. The ever-increasing environmental pollution and the abuse of antibiotics further greatly challenged the global water security-related issues. Therefore, the development of high-efficiency, low-cost disinfection technologies should be constantly emphasized. Conventional water disinfection technologies (e.g. chlorination, ozonation and UV irradiation, etc.) although were extensively used and exhibited acceptable efficiency, they also suffered from unavoidable drawbacks (carcinogenic byproducts, recolonization and high energy input, etc.). Developing alternative disinfection technologies with high efficiency and low energy consumption is therefore urgently and valuable, but also challengeable in scientific community (An et al., 2016).

Using inexhaustible solar energy only to disinfect water, an alternative green and energy-saving method, when used properly, was demonstrated to be practicable to ensure the water quality in regions with plentiful sunlight (Keane et al., 2014). However, the low efficiency, the need for sufficient sunlight and the small volume of treated water limited the wide application of this solar energy-only method. The semiconductor-based solar-driven photocatalytic disinfection method, an update version of solar-driven disinfection, offers real possibilities for eliminating lethal pathogenic microorganisms from drinking water, as the photocatalytic process can obviously accelerate the bacterial inactivation rate by the photogenerated reactive species (Keane et al., 2014; Wu et al., 2015; Xiao et al., 2020; Sun et al., 2019; Xia et al., 2015, 2018; Wu et al., 2015; Xia et al., 2015, 2018). For example, as compared to the poor inactivation efficiency of pure photocatalysis process without semiconductor photocatalysts, the elemental photocatalyst red phosphorus showed dramatically enhanced efficiency to inactivate *Escherichia coli* under visible light irradiation, owing to the promotion effects of the reactive oxygen species derived from the photogenerated carriers (Xia et al., 2015). However, even though the photocatalytic disinfection method has received enormous attention and shown great promising, the light response range of most identified photocatalysts are extended to visible light (VL) only. They cannot make full utilization of the whole solar spectrum, not to mention those catalysts response to UV only. Given the UV and VL occupy only 5% and 45% of the solar spectrum, while infrared light constitutes about 50% of the solar spectrum, efforts started to be devoted to pursuing NIR/IR-responsive photocatalysts in recent years (Tian et al., 2013; Li et al., 2012, 2018; Sang et al., 2015; Qin et al., 2010; J. Li et al., 2019; B. Li et al., 2019; Li et al., 2018; Xu et al., 2020). For example, Wu et al. developed a NIR-active photocatalytic platform composed of an upconversion nanocrystals shell and an Au/dark-TiO_2 core, which can efficiently inactivate ampicillin sodium - resistant bacteria strains. The Au surface-plasmon resonance on dark TiO_2 guaranteed the upconversion of NIR into green light, contributing to the NIR-triggered antibacterial activity (Xu et al., 2020). Although some successful NIR driven photocatalystic systems are developed recently for bacterial inactivation (B. Li et al., 2019; Xu et al., 2020; Lin et al., 2019; Gorle et al., 2018; X. Zhang et al., 2020; Zhang et al., 2018; Q. Zhang et al., 2020; Sun et al., 2019), noble metals (i.e. Au (B. Li et al., 2019; Xu et al., 2020), Ag (Lin et al., 2019)) are highly involved to enhance the inactivation efficiency, which would inevitably increase the disinfection cost. Therefore, to maximize the utilization rate of solar energy and minimize the cost, it is highly desirable to develop non-precious metal photocatalysts with broader solar spectral response (e.g., UV to NIR region) for bacterial inactivation. The vacancy rich BiO_{2-x} is a promising NIR directly responsive semiconductor (B. Li et al., 2019; Li et al., 2018), which has already shown photocatalytic degradation ability toward Rhodamine B and phenol even under NIR irradiation (Li et al., 2018). We recently also found that the yolk-shell BiO_{2-x} has potential to inactivate *Escherichia coli* (*E. coli*) under visible light irradiation (Sun et al., 2018). The rich vacancy presented in BiO_{2-x} facilitated the trap of photogenerated electrons and formation of O_2^-, promoting the photocatalytic activity. However, the photocatalytic efficiency is yet not satisfactory for practical use, thus additional technologies are required to elevate the disinfection efficiency.

Intrinsically, the bacterial inactivation relied on the oxidizing power of reactive species. In most photocatalytic disinfection system, the generated effective reactive radicals are ·OH, O_2^- and h^+, etc. However, they possessed quite short life span in water, limiting the sterilization rate to a certain extent. In contrast, the sulfate radicals ($\cdot SO_4^-$) possessed oxidizing power comparable to ·OH, but are much more stable in solution. Actually, the $\cdot SO_4^-$ based advanced oxidation process (AOP) has been demonstrated to be useful in organic pollutants degradation (Lee et al., 2020; Khan et al., 2017; Anipsitakis and Dionysiou, 2003; Lutze et al., 2015; Antoniou et al., 2010). For bacterial inactivation, $\cdot SO_4^-$ also exhibits a huge potential (W. Wang et al., 2019; Yu et al., 2021; Wang et al., 2020). For example, Yu et al. found that the mutual interaction between sulfidated nano-zerovalent iron and persulfate (PS) could initiate the decomposition of PS to $\cdot SO_4^-$. The formed $\cdot SO_4^-$ thus played a significant role in quickly eliminating the pathogenic bacteria (Yu et al., 2021). Wang et al. also successfully decomposed PS into $\cdot SO_4^-$ by VL irradiation, and obtained satisfactory disinfection activity (W. Wang et al., 2019). Hence, the introduction of $\cdot SO_4^-$ into the photocatalytic system would highly possibly further promote the disinfection efficiency for real practical application. Generally, the sulfate radicals can be formed through light activation (Khan et al., 2017; W. Wang et al., 2019; Lau et al., 2007), heat activation (Tan et al., 2012; Gu et al., 2011), or metal-catalyzed activation method (Anipsitakis and Dionysiou, 2003; Yu et al., 2021). As for the light activation method (energy transfer reaction), unfortunately, most focused on the UV or VL irradiation, overlooking that NIR irradiation might be a good alternative and more cost-effective activation method. For heat activation method (energy transfer reaction), it is reported that only when the temperature reached up to 50 °C, the PS can be efficiently decomposed into $\cdot SO_4^-$ for effective bacterial inactivation (W. Wang et al., 2019). Differently, the principles behind the metal-catalyzed activation were electron transfer reactions, those reduction metals/metal oxides (Fe (Yu et al., 2021) and Co (Anipsitakis and Dionysiou, 2003), etc.) transferring electrons to PS for generating $\cdot SO_4^-$. Besides, the photogenerated-electrons in photocatalytic system can also activate PS through electron transfer reactions. In this regard, when the $\cdot SO_4^-$ based AOP is combined with NIR-driven semiconductor-based photocatalytic process, both energy and electron transfer reactions can take effect to synergistically produce powerful reactive radicals for bacterial disinfection. However, the synergistic effect between NIR-driven photocatalysis and PS activation for bacterial inactivation has not been well investigated. Therefore, it is attractive to develop a distinctive combined system that can catalyze the PS decomposition through multiple ways and can also act as a NIR-responsive photocatalytic system for bacterial inactivation.

Herein, vacancy-rich BiO_{2-x} nanosheets were firstly synthesized using a facile one-step hydrothermal method, then collaborated with PS activation forming a novel NIR responsive collaboration system. The bacterial inactivation performances of the novel collaborating system under NIR ($\lambda > 700$ nm) light irradiation were studied in detail, with sufficient reactive sulfate radicals formed via multiple channels, which finally completely inactivated 7 logs of the *E. coli* within 40 min. Moreover, the bacterial inactivation mechanisms related to primary reactive species, cell morphology change, antioxidant enzyme activity

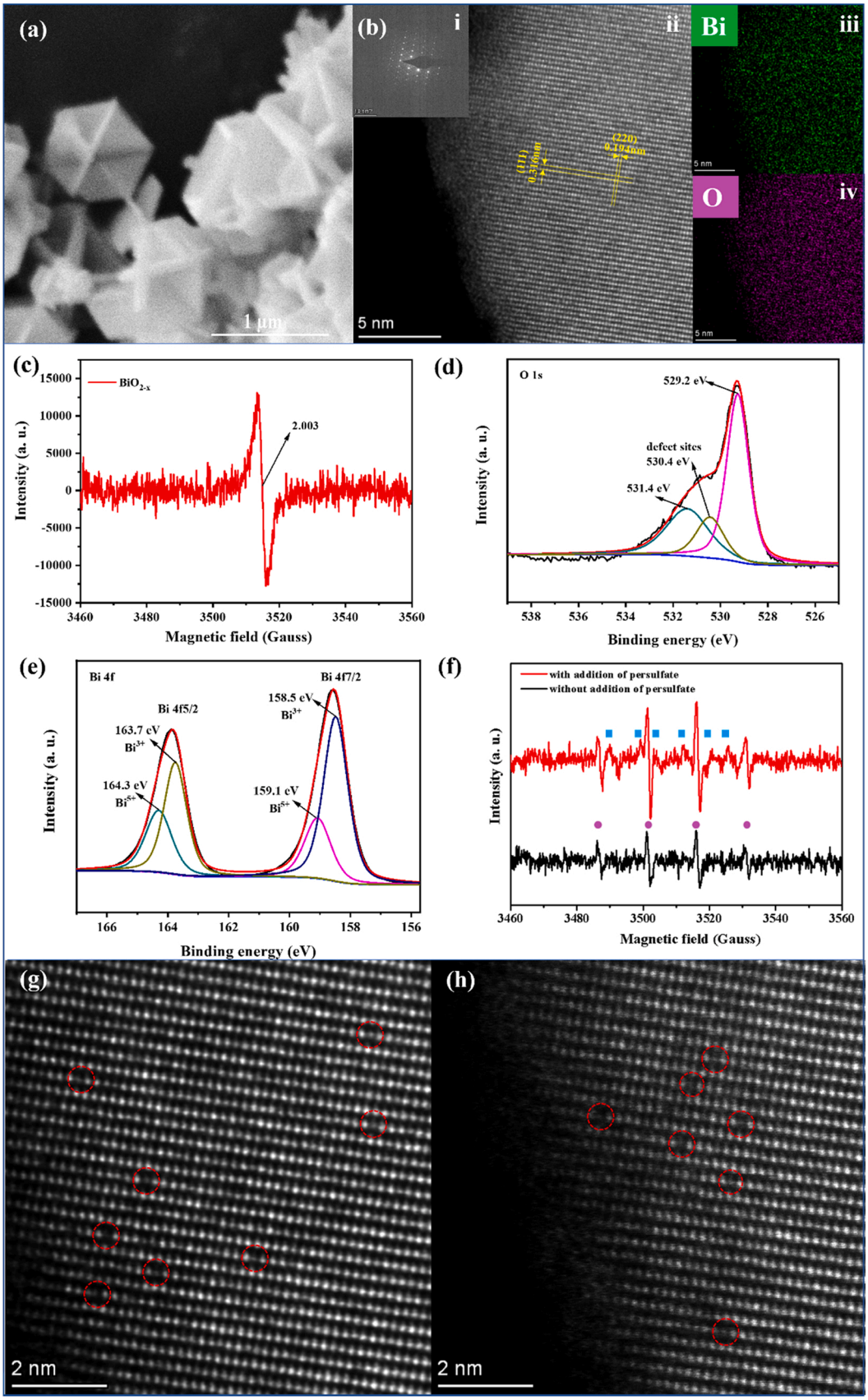

Fig. 1. (a) SEM image, (b) HRTEM images (i: SAED image; ii: lattice fringes; and element mapping of (iii) Bi and (iv) O.), (c) low temperature EPR, high resolution (d) O 1s and (e) Bi 4f core-level XPS spectrum, (f) EPR signals (purple circles: hydroxyl radicals; blue cubes: sulfate radicals) of the collaborating system with/without addition of persulfate under NIR irradiation. (g, h) Spherical aberration correction transmission electron microscope images of BiO_{2-x}.

and chromosomal DNA destruction were systematically investigated. This work may provide a new route for developing a low-cost collaborating system to fully utilize inexhaustible energy in solar spectrum for bacterial inactivation.

2. Material and methods

2.1. Synthesis of BiO_{2-x} nanoplates

The defective BiO_{2-x} nanoplates were fabricated using a simple hydrothermal method. In a typical preparation procedure, the sodium bismuthate ($NaBiO_3{\cdot}2H_2O$, 12 mmol, Sinopharm Chemical Reagent Co., Ltd, AR grade) and the ammonium dihydrogen phosphate ($NH_4H_2PO_4$, 12 mmol, Sinopharm Chemical Reagent Co., Ltd, AR grade) were added into the NaOH solution (1 M, 60 mL) firstly, followed by continuous stirring for 30 min. Then the obtained suspension was transferred and hydrothermally treated at 220 °C for 6 h in a 100 mL *p*-polyphenylene-based stainless steel autoclave. After the reaction, the red-brown precipitates were collected, washed several times with deionized water, and finally dried at 60 °C.

2.2. Characterization of BiO_{2-x} nanoplates

X-ray diffraction (XRD) patterns for the as-prepared samples were determined by a Rigaku Smartlab X-ray diffractometer (Japan) with CuKα source irradiation (l=1.5406 Å, 40 kV, 40 mA). The Raman was tested on Scientific LabRAM HR Evolution (Horiba, Japan). The FTIR spectrum was measured by Vertex70V (Bruker, Germany). The microscopic images were characterized by scanning electron microscopy (SEM) on a FEI Quanta 400 microscope (FEI, USA). Electron paramagnetic resonance (EPR) spectroscopy was performed with a JES FA200 spectrometer (Jeol, Japan). The high resolution transmission electron microscopy (HRTEM), selected area electron diffraction image (SAED) and aberration corrected TEM images were performed on Titan Cubed Themis G2 300 (FEI, USA). X-ray photoelectron spectra (XPS) and valence band XPS spectra of the samples were recorded on ESCALAB 250Xi apparatus (Thermo Fisher Scientific, USA) with AlKa radiation (1486.6 eV) X-ray sources. The obtained spectra were calibrated with reference to the binding energy of C1s (284.8 eV) and all peaks were well fitted by "XPSPEAK" analysis software. The light absorption abilities of the samples were determined by UV/Vis diffuse reflectance spectroscopy over a range of 200–2000 nm on a PerkinElmer Lambda 950 spectrometer (PerkinElmer, USA).

2.3. Near infrared (NIR) driven photocatalytic bacterial inactivation

The Gram-negative bacterium, *E. coli* K-12, was chosen as the model bacterium for mechanism study in this study. Firstly, the bacterial cells were harvested by centrifugation (13,000 rpm, 1 min, MiniSpin, Eppendorf, Germany) after incubation at 37 °C for 16 h in 50 mL of nutrient broth (Lab M, Lancashire, U.K.). Then the collected cell pellet was washed twice with sterilized saline (0.9% NaCl) solution and resuspended in the same volume of sterilized saline solution for use. Secondly, the cell density of the reaction solution was adjusted to be 10^7 cfu/mL by uniformly dispersing 200 μL of the above freshly made bacterial suspension into 25 mL sterilized saline solution. Then, 20 mg of the catalysts and a certain amount of persulfate solution were added to the mixture, of which the final concentration of persulfate ($K_2O_8S_2$) was 3 mM. Finally, a 300 W Xenon lamp (PLSSXE300C, Beijing Perfect Light Technology Co., Ltd. China) equipped with a 700 nm cutoff filter was adopted as the NIR light source to illuminate the mixture and initiate the reaction. At fixed time intervals, aliquots of the sample were collected, serially diluted, immediately spread on the nutrient agar (Lab M, Lancashire, U.K.) plates, and then incubated at 37 °C for 24 h to determine the survival number of cells (in cfu). All the bacterial disinfection experiments were conducted in triplicate.

2.4. Mechanism analysis methods

2,3,5-triphenyl tetrazolium chloride (TTC) was used as a substrate to evaluate the cellular respiration activity by a colorimetric measurement. The concentration of the red formazan, which was reduced from TTC, was monitored by measuring the absorption at 460 nm. The ATP synthesis ability of the bacterial cells was evaluated according to ATP Detection Assay Kit-Luminescence (Cayman Chemical, Item No. 700410, USA). The superoxide dismutase (SOD) and catalase (CAT) activity were assessed by using the Superoxide Dismutase Assay Kit (Cayman Chemical, Item No. 706002, USA) and the Catalase Assay Kit (Cayman Chemical, Item No. 707002, USA), respectively. Protein Carbonyl Colorimetric Assay Kit (Cayman Chemical, Item No. 10005020, USA) was applied to determine the levels of protein carbonyl. And the peroxidation extent of the lipid was investigated via the Lipid Hydroperoxide (LPO) Assay Kit (Cayman Chemical, Item No. 705003, USA). The DNA and RNA leakage were measured with a Nanodrop spectrophotometer (Thermo Nanodrop One, USA). The fluorescent staining experiment was assayed according to the LIVE/DEAD BacLight Bacterial Viability Kit (Molecular Probes, Item No. L7012, USA). The direct observation of membrane destruction was monitored by SEM. Firstly, the treated and untreated cells were harvested and fixed with 5% glutaraldehyde solution for 4 h. After washed by phosphate buffer solution, the cell suspension was transferred to lysine pre-coated FTO (Fluorine-doped Tin Oxide). The obtained FTO (loaded with cells) were then dehydrated in the gradient ethanol (50% EtOH, 10 min; 70% EtOH, 10 min; 85% EtOH, 10 min; 95% EtOH, 10 min, twice; 100% EtOH, 10 min, three times.) and subjected to the critical point drying (LADD 28002, USA). Finally, the cell membrane was observed with a SEM (FEI Quanta 400 F, USA) after gold-sputtering.

For the β-D-galactosidase activity assay, 1 mL of incubated *E. coli* suspension (nutrient broth, 16 h) was recultured in 100 mL of nutrient broth containing 1 mM isopropyl *β*-D-thiogalactopyranoside (IPTG) to induce the synthesis of *β*-D-galactosidase (37 °C, 200 rpm, 4 h). Induced cells were harvested for studying the catalytic inactivation efficiency. Aliquots of 0.5 mL samples were collected at regular time, mixing with 0.5 mL 2x PBS. Before addition of o-nitrophenyl-*β*-D-galactopyranoside (ONPG), the mixture can be permeabilized or not by adding SDS (sodium dodecyl sulfate, one drop) and chloroform (two drops) or not. The final ratio of them on the ONPG hydrolysis activity can reflect the membrane permeability. Then, 0.2 mL of 5 mM was added to the mixture to initiate the reaction. The reaction was kept at 37 °C with vibration for 60 min, then ended by adding 0.5 mL Na_2CO_3 (1 M). The absorbance at both 420 nm and 550 nm were measured. The ONPG hydrolysis rate (nmol min^{-1} mL^{-1}), namely, the *β*-D-galactosidase enzyme activity was calculated based on the following equation.

$$\text{ONPG hydrolysis rate} = \frac{A_{420}-A_{550}}{T\times\varepsilon_{ONP}} \times \frac{1.7mL}{0.5mL}.$$

ε_{ONP} represents the molar absorption coefficient of o-nitrophenol (ONP, A_{420}/nM), T is the total enzymatic reaction time (min).

3. Results and discussion

3.1. Characterization of materials

The sharp peaks of the as-synthesized sample in XRD pattern (Fig. S1) were well indexed to the cubic phase BiO_{2-x} with JCPDS No. 47-1057 (Li et al., 2018), indicating the successful preparation of pure phase BiO_{2-x} with good crystallinity. Both Raman (Fig. S2) and FTIR spectra (Fig. S3) showed characteristic peaks of BiO_{2-x}, further demonstrating the successful preparation of BiO_{2-x}. As shown in the SEM image, the synthesized BiO_{2-x} were hierarchically structure assembled by nanoplates (Fig. 1a). SAED pattern implied the single-crystal nature (Fig. 1b-i) of BiO_{2-x}. And HRTEM clearly revealed the BiO_{2-x} with good crystallinity possessed lattice fringe spacing of 0.316 and 0.194 nm, corresponding to the (111) and (220) lattice planes

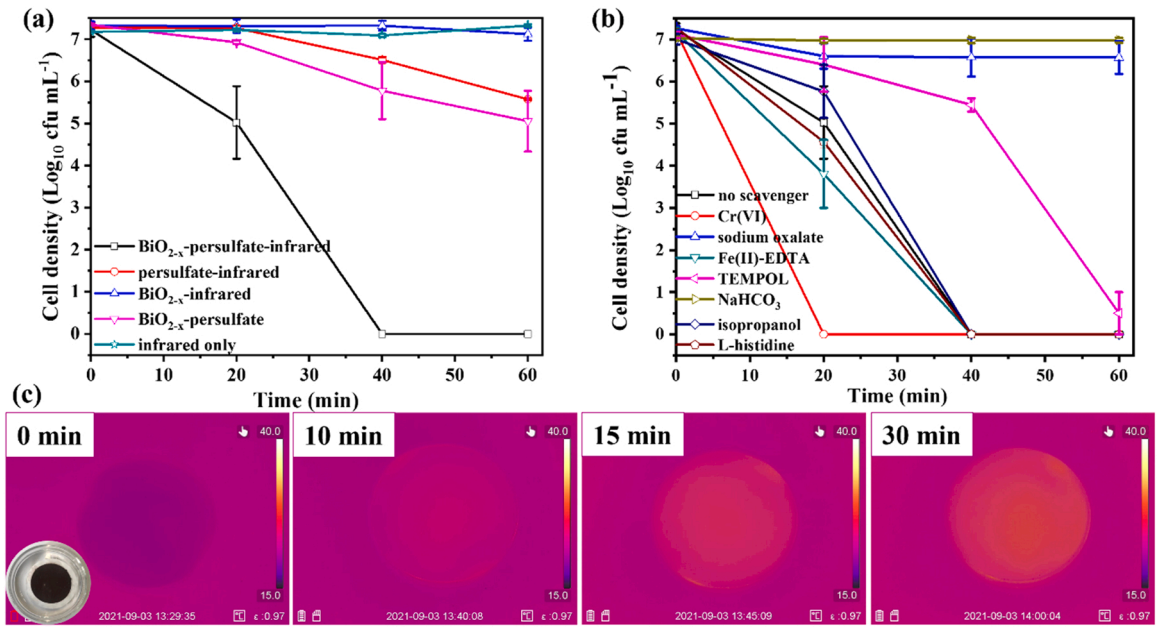

Fig. 2. (a) The *E. coli* inactivation performance, and (b) the corresponding scavenger studies of the collaboration system under NIR irradiation. (c) The thermal imaging of BiO_{2-x} under NIR irradiation ($\lambda > 700$ nm).

of BiO_{2-x}, respectively (Fig. 1b-ii). The elemental mapping confirmed the homogeneous distribution of Bi and O elements within the nanoplates (Fig. 1b). These BiO_{2-x} nanoplates possessed impressive light absorption ability, of which the absorption range was broaden to even near infrared region (around 800 nm, Fig. S4) and the band gap was calculated to be 1.34 eV (Fig. S5), implying their promising applications in NIR driven photocatalysis. The photocurrent response under NIR irradiation also indicated its potential NIR-driven photocatalytic activity (Fig. S6). The low temperature (77 K) electron paramagnetic resonance (EPR) analysis (Fig. 1c) of the BiO_{2-x} nanoplates showed an apparent peak with *g*-value at 2.003, revealing the rich vacancy feature within the BiO_{2-x} structure (Sun et al., 2018; Li et al., 2017, 2014). Besides, the existence of the rich vacancy was further evidenced by the XPS analysis and aberration corrected TEM analysis (AC-TEM). For O 1 s core-level spectra of BiO_{2-x} (Fig. 1d), apart from the peak at 529.2 eV related to the lattice oxygen bound to metals, a new deconvoluted peak at 530.4 eV was identified, which was attributed to a high number of defect sites with low oxygen coordination (Bao et al., 2015). And the peak at 531.4 eV resulted from the hydroxyl groups or surface-adsorbed oxygen. Yang et al. (2019) The Bi 4f spectra (Fig. 1e) were characterized by four peaks, including a spin doublet (4f7/2 and 4f5/2) of Bi^{3+} at 158.5 and 163.7 eV, and a doublet of Bi^{5+} at 159.1 and 164.3 eV, respectively. Besides, the direct observation of a lot of vacancy sites in different areas through AC-TEM images (Fig. 1g, h), further demonstrating the rich vacancy feather of as-synthesized BiO_{2-x} nanoplates. These vacancy-rich BiO_{2-x} nanoplates can efficiently activate persulfate to form the sulfate radicals under NIR irradiation. As shown in Fig. 1f, the NIR irradiation of the water suspension of BiO_{2-x} only can induce the formation of hydroxyl radicals. In contrast, when the water suspension of BiO_{2-x} powders, persulfate and DMPO trapping agent was irradiated by the NIR light for 10 min, both the signals of the hydroxyl radicals and the sulfate radicals were identified, indicating that the vacancy-rich BiO_{2-x} was a high-efficient persulfate activator to form active sulfate radicals under NIR irradiation. The ESR test also convinced the presence of the hydroxyl radicals and the sulfate radicals in the collaborating system during the inactivation process.

3.2. Bacterial inactivation efficiency

Such NIR-sensitive BiO_{2-x} nanosheets have shown great promise in activating persulfate for sterilizing bacteria under NIR irradiation. Fig. 2a displayed the variations of *E. coli* cell densities as a function of reaction time in various catalytic conditions. It can be found that around 7 logs of the *E. coli* could be completely inactivated within 40 min by the BiO_{2-x} based collaboration system under NIR irradiation ($\lambda > 700$ nm), which showed comparable and even much better performance than those published studies (Table S1). Even in the phosphate buffered saline solution, the 7 logs of *E. coli* could still be completely inactivated within 60 min, demonstrating the superior bacterial inactivation performance of our collaborating system (Fig. S7). However, the *E. coli* cells were highly resistant and tenacious when any specific factor was excluded from the collaborating system. The sole activation of persulfate by NIR ($\lambda > 700$ nm) irradiation could only achieve about 1.5 logs of cell loss, suggesting that the NIR irradiation induced heat or light activation of persulfate indeed existed, but apparently insufficient in the bacterial disinfection process (*E. coli* cell density: 10^7 colony forming units). Besides, if there was no NIR irradiation, the synergy effect between BiO_{2-x} and persulfate also existed, but limited and unsatisfactory, which obtained less than 2 logs of cell loss at the initial stage and would regain their activity (Fig. S8). Only when BiO_{2-x} nanoplates, persulfate and NIR irradiation cooperated within a collaboration system, the persulfate can be efficiently activated to generate sulfate radicals (Fig. 1f). This is because, on one hand, BiO_{2-x} nanoplates can be excited by NIR to generate carriers for PS activation through electron transfer reaction, on the other hand, BiO_{2-x} can promote the heat absorption of the collaboration system for PS activation through energy transfer reaction. The thermal imaging under NIR irradiation (Fig. 2c) clearly revealed the positive effects of BiO_{2-x} on promoting the heat absorption. The formed sulfate radicals supplemented with some other oxidative radicals, forming a powerful disinfection system and causing the complete inactivation of ∽ 7 logs of the *E. coli* within 40 min. To figure out whether the cells treated by the collaborating system would self-repair and regrow, the treated cells were re-cultured under nutrient broth for 24 h. However, no colony was found based on the plate counting method (Fig. S9d), demonstrating the complete death rather than the dormancy of the bacteria cells. Moreover, the performance stability and structure

tolerance of vacancy-rich BiO_{2-x} were also studied in detail. As shown in Fig. S10, the bacterial cells were all efficiently inactivated within 40 min in four repeat cycles, suggesting the vacancy-rich BiO_{2-x} can be reused without loss of activity. Besides, there was negligible change in the XRD pattern between the used BiO_{2-x} and their pristine counterpart, implying that the structure of BiO_{2-x} was quite stable. In addition, as indicated by both ESR and XPS characterizations, the rich-vacancy features were still well preserved after cycling experiments, further indicating the superior structure endurance of BiO_{2-x} for collaborating with persulfate to inactivate *E. coli* cells under NIR irradiation.

3.3. Bacterial inactivation mechanisms and cell damage process

3.3.1. Scavenger study

To comprehensively understand the bacterial inactivation mechanism of the efficient collaboration system, the scavenger studies were firstly conducted to investigate the key reactive species and their contributions (Fig. 2b). The concentration of each applied scavenger was optimized ahead to ensure the scavenging effect but no toxic or inactivation effect to the bacterial cells. The scavengers used in this study were sodium oxalate (0.5 mM) for h^+, ·OH and $\cdot SO_4^-$. Cr(VI) (0.1 mM) for e^-, TEMPOL (1 mM) for O_2^-, Fe-EDTA (0.1 mM) for H_2O_2, isopropanol (7.5 mM) for ·OH and $\cdot SO_4^-$, and $NaHCO_3$ (0.1 M) for ·OH and $\cdot SO_4^-$. As seen in Fig. 2b, after introducing different scavengers, the inactivation efficiency was affected differently. Sodium oxalate was a commonly used hole scavenger as depicted in Eq. (1) (Bangun, 1998). In fact, sodium oxalate was also an efficient scavenger of ·OH (Eq. (2)) and $\cdot SO_4^-$ (Eq. (3)), but it is often overlooked, with reaction rate constant up to 10^6 (Huie and Clifton, 1996). The dramatic inhibition by the sodium oxalate indicated the great significance of either photogenerated h^+, ·OH or $\cdot SO_4^-$ in the disinfection process. The poor inactivation efficiency of pure photocatalytic system (BiO_{2-x}+NIR irradiation) seemed to rule out the importance of h^+. However, the poor efficacy of the pure photocatalytic system might be due to the fast recombination of e^- and h^+. The reaction between Cr (VI) and e^- can inhibit the recombination of the electrons and holes, releasing h^+ for redox reactions. The addition of the Cr (VI) to both the pure photocatalytic system (BiO_{2-x}+ NIR irradiation, Fig. S11) and the collaboration system (BiO_{2-x}+NIR irradiation + persulfate, Fig. 2b) promoted the inactivation efficiency, indicating that the photogenerated holes indeed made a difference to disinfection activity in the collaboration system. Especially, in addition to facilitating the dissociation of $S_2O_8^{2-}$ to $\cdot SO_4^-$, the extremely fast reaction between e^- and persulfate (Eq. (4)) (Huie and Clifton, 1996) also made the persulfate of the system acting as an excellent e^- scavenger for releasing holes. All of this convinced the importance of h^+ in guaranteeing the sterilization effectiveness of the collaboration system.

Similarly, the addition of $NaHCO_3$ also strikingly suppressed the damage to bacterial cells, as the oxidative species with strong oxidative ability, ·OH (2.8 V) and $\cdot SO_4^-$ (2.7 V), were efficiently trapped by $NaHCO_3$ (Eqs. (7)–(9)) (Khan et al., 2017; Tan et al., 2012; Gu et al., 2011; Kochany and Kochany, 1992). Given the reaction kinetics between $NaHCO_3$ and ·OH ($(5.7–8.5) \times 10^6\ M^{-1}\ S^{-1}$) and $\cdot SO_4^-$ ($(2.8–9.1) \times 10^6\ M^{-1}\ S^{-1}$) were similar (Khan et al., 2017; Tan et al., 2012), isopropanol was applied additionally to distinguish their effects. Isopropanol exhibited higher reactivity towards ·OH ($k_{isopropanol\ -\ hydroxyl}$: $1.9 \times 10^9\ M^{-1}\ S^{-1}$) than $\cdot SO_4^-$ ($k_{isopropanol\text{-}sulfate}$: $4.0 \times 10^7\ M^{-1}\ S^{-1}$) (Lee et al., 2020; W. Wang et al., 2019; Ahmad et al., 2013). Hence, when isopropanol was presented into the system, ·OH tended to be trapped rather than $\cdot SO_4^-$, owing to the faster reaction rate. With addition of isopropanol, a slight reduction of the inactivation rate was observed, implying the unneglected role of ·OH in the reaction. But the role is a little bit limited, possibly because of the relatively low concentration of short-lived ·OH formed in the process. As compared to the significant inhibition from $NaHCO_3$, the finally almost unchanged efficiency in the system with isopropanol suggested that, $\cdot SO_4^-$ was much more important as one of the major reactive species and responsible for the inactivation of *E. coli*. The formation pathway of $\cdot SO_4^-$ in this collaboration system can be summarized as the following three types. The NIR irradiation induced light or heat dissociation way (Eqs. (5)–(6)) (Antoniou et al., 2010; Lau et al., 2007; Tan et al., 2012) and the dissociation mode by persulfate reacting with photogenerated e^- (Eq. (4)).

Moreover, the slight promotion induced by the addition of Fe-EDTA was mainly ascribed to the interaction between the $\cdot SO_4^-$ and H_2O_2 (Eq. (12)) (Lau et al., 2007). When H_2O_2 was eliminated by the corresponding scavenger, more $\cdot SO_4^-$ was able to take part in the inactivation process. The elimination of O_2^- by TEMPOL also alleviated the sterilization effect obviously, implying the positive role of the O_2^- in this collaboration system. Comparing with the O_2^- signals of the pure BiO_{2-x} suspension under NIR irradiation, the collaboration system showed enhanced O_2^- signals according to the ESR analysis (Fig. S12), revealing that the superoxide radicals were formed in multiple ways. Some O_2^- were formed through the reaction between the dissolved oxygen with the photogenerated electrons (Eq. (13)) (Huie and Clifton, 1996; Huang et al., 2020), which was thermodynamically feasible according to the calculated band structure of BiO_{2-x} (Fig. S13, 14). Some were from the transformation of persulfate ions, as shown in Eqs. (10)–(11) (Ahmad et al., 2013). So, as for the collaboration system, it is the $\cdot SO_4^-$ that acted as the primary reactive species to sterilize the bacterial cells, accompanied by the promotion effects of O_2^-, h^+ and ·OH radicals.

$$h^+ + C_2O_4^{2-} \rightarrow \bullet C_2O_4^- \quad (1)$$

$$\cdot OH + C_2O_4^{2-} \rightarrow \cdot C_2O_4^- + OH^- \quad k = 7.7 \times 10^6 M^{-1}S^{-1} \quad (2)$$

$$\cdot SO_4^- + C_2O_4^{2-} \rightarrow \cdot C_2O_4^- + SO_4^{2-} \quad k = 5.6 \times 10^6 M^{-1}S^{-1} \quad (3)$$

$$e^- + S_2O_8^{2-} \rightarrow \cdot SO_4^- + SO_4^{2-} \quad k = 1.2 \times 10^{10} M^{-1}S^{-1} \quad (4)$$

$$S_2O_8^{2-} \xrightarrow{heat} 2\bullet SO_4^- \quad (5)$$

$$S_2O_8^{2-} \xrightarrow{light} 2\bullet SO_4^- \quad (6)$$

$$\cdot SO_4^- + HCO_3^- \rightarrow H^+ + \cdot CO_3^- + SO_4^{2-} \quad k = (2.8 - 9.1) \times 10^6 M^{-1}S^- \quad (7)$$

$$\cdot SO_4^- + HCO_3^- \rightarrow \cdot HCO_3 + SO_4^{2-} \quad k = 1.6 \times 10^6 M^{-1}S^{-1} \quad (8)$$

$$\cdot OH + HCO_3^- \rightarrow \cdot CO_3^- + H_2O \quad k = (5.7 - 8.5) \times 10^6 M^{-1}S^{-1} \quad (9)$$

$$H_2O + S_2O_8^{2-} \rightarrow \bullet HO_2^- + 2SO_4^{2-} + H^+ \quad (10)$$

$$\bullet HO_2^- + S_2O_8^{2-} \rightarrow O_2^- + \bullet SO_4^- + SO_4^{2-} + H^+ \quad (11)$$

$$\bullet SO_4^- + H_2O_2 \rightarrow H^+ + \bullet HO_2 + SO_4^{2-} \quad (12)$$

$$O_2 + e^- \rightarrow O_2^- \quad k = 1.9 \times 10^{10} M^{-1}S^{-1} \quad (13)$$

To sum up, in the novel collaboration system, the synergy between BiO_{2-x} and NIR irradiation are multiple, exerting impressive effects on the system. On one hand, the NIR irradiation itself can induce the transformation of persulfate to sulfate radicals though light and heat activation mode directly (Eqs. (5) and (6)). In the meantime, the heat absorption capacity of NIR responsive BiO_{2-x} would further increase the temperature of the system, promoting the decomposition of persulfate to sulfate radicals. On the other hand, the NIR irradiation could activate BiO_{2-x} to generate active holes and electrons for photocatalytic redox reactions. The persulfate can be quickly reduced by the photogenerated electron to produce one sulfate radical and one sulfate ion (Eq. (4)). Therefore, the activation of persulfate in the collaboration system is multi-channel, guaranteeing the sufficient effects of sulfate radicals on the *E. coli* disinfection. Furthermore, the generated O_2^-, h^+ and ·OH reactive species acted synergistically with sulfate radicals for well-

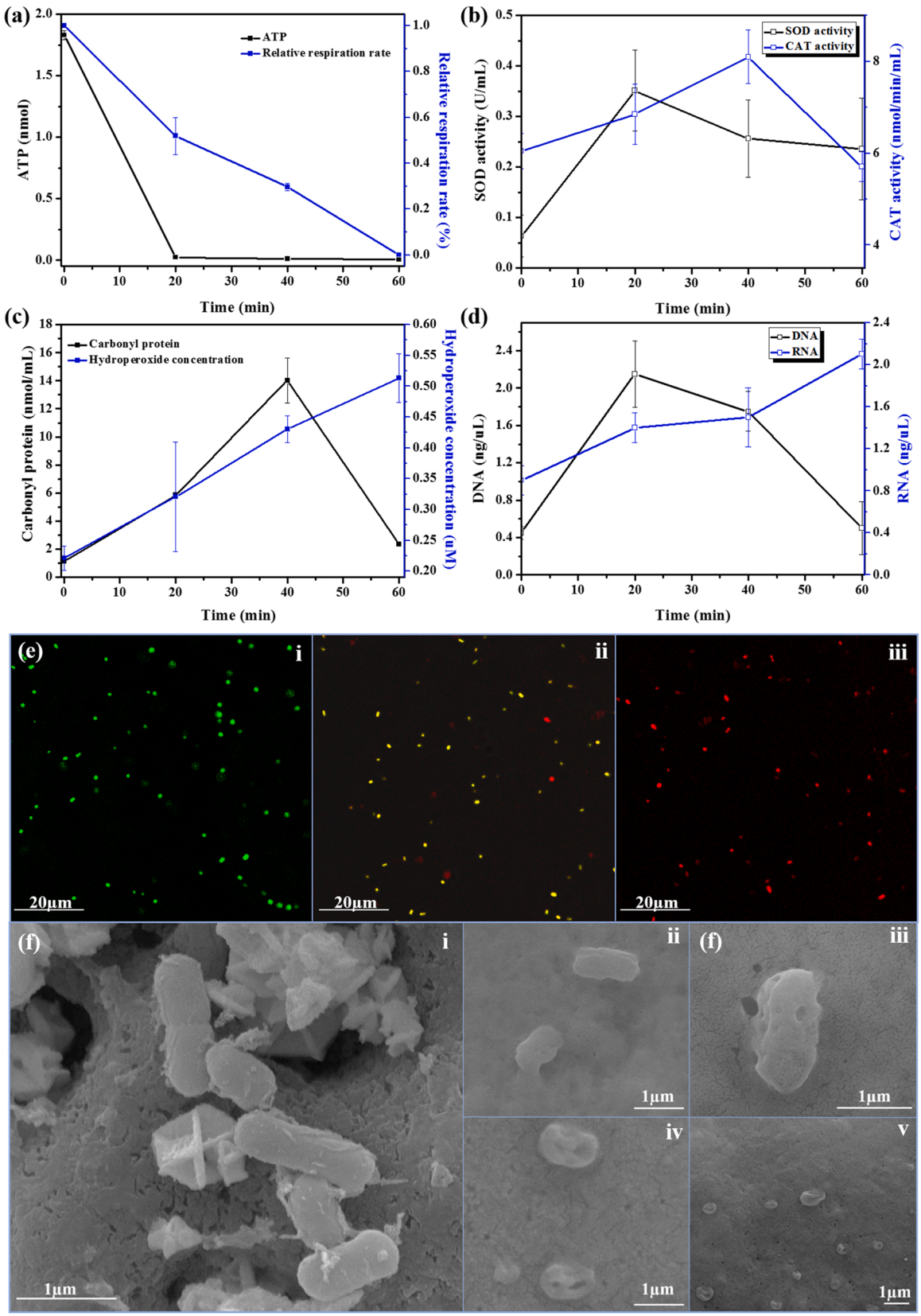

Fig. 3. (a) ATP synthesis and cell respiration, (b) SOD and CAT activity, (c) protein carbonyl and lipid peroxidation level, and (d) the leakage of DNA and RNA during bacterial destruction process. (e) Fluorescence microscopy images of *E. coli* cell (i: without treatment; ii: treated for 30 min; iii: treated for 60 min). (f) SEM images of *E. coli* cells after treated by the collaboration system for (i) 0 min, and (ii, iii, iv and v) 60 min.

performed sterilization process.

3.3.2. Analysis of cell damage process

To better understand the underlined inactivation mechanism of the collaboration system, a comprehensive and in-depth investigation of the bacterial cell damage processes was conducted. Superoxide dismutase (SOD) and catalase (CAT) are two types of significant antioxidant enzymes, involved in the self-protective system. They catalyze the conversion of the reactive species (RSs) and detoxify them, effectively eliminating or mitigating the damage to the cells. Specifically, SOD can disproportionate $\bullet O_2^-$ to O_2 and H_2O_2, and CAT catalyze H_2O_2 to O_2 and H_2O (Xiao et al., 2020; W. Wang et al., 2019; Wang et al., 2020; Sun et al., 2014; Chen et al., 2011). Thus, both SOD and CAT play key roles in protecting the cells from those RS-induced oxidative damages. Here, the activity of SOD and CAT were investigated firstly. As shown in Fig. 3b. They both increased at the initial stage and then decreased during the inactivation process. The observed increment of the activity of SOD and CAT at the beginning indicated an activation of self-protection system when attacked by RSs. So, the SOD and CAT activities were stimulated to increase for a short period. As the inactivation process progresses, those generated RSs with great attack potential accumulated and overwhelmed the limited defense capabilities of enzymes. Therefore, the antioxidant enzymes were severely damaged and lost their activity gradually.

In bacterial cells, the evaluation of the respiration activity by assaying electron transport system (ETS) activity can provide a suitable measure of cell metabolic activity. The bacteria cells with active ETS can reduce water soluble tetrazolium salts (e.g. 2,3,5-triphenyl tetrazolium chloride (TTC)) to colored, water insoluble formazan products (Xia et al., 2015; B. Wang et al., 2019; Maness et al., 1999). This property can be applied as an indicator for the quantitative measurement of the respiration activity of bacteria. As shown in Fig. 3a, the respiration rate of *E. coli* cells kept falling drastically with increasing NIR irradiation time, indicating that with the collapse of the oxidative defense system, the enzymes in ETS and metabolism collapsed as well. And the dysfunction of the ETS implied they could no longer maintain the redox potential and produce protons for energy production (e.g. ATP synthesis). ATP is the main biological energy currency in the cell, which is synthesized through the oxidation of substrate driven by the proton motive force produced in the respiration chain (Xiao et al., 2020; Xia et al., 2015; Maness et al., 1999). As expected, the ATP level decreased dramatically (Fig. 3a), suggesting the severe functional inactivation of membrane-bounded ATPase and the destruction of bacterial energy metabolism.

The functional inactivation of ETS, ATPase and the associated poor energy metabolism showed the damages are at the energy metabolism functional level. It is also essential to deeply investigate the damages at the membrane structure level to reveal whether the RSs generated from the collaboration system caused the membrane disintegration. Thus, the oxidation extent of the cellular building blocks such as proteins and lipids were evaluated to reflect the disintegration of membranes. The lipids of the cell membrane are responsible for the fluidity and permeability of membrane bilayer (Gaschler and Stockwell, 2017; Catala and Diaz, 2016). Lipid peroxidation indicates the oxidative injury in pathophysiological disorders, and can result in the formation of highly reactive and unstable hydroperoxides of both saturated and unsaturated lipids. So the estimation of lipid hydroperoxide level reflects the lipid peroxidation (LPO) level. The consistent growth of LPO level in Fig. 3c demonstrated the impairment of diffusion ability and the fragmentation of the bilayer.

Normally, the fragmentation of the phospholipid bilayer would accompany with the increment of nonspecific permeability of the membrane. To further reveal the effects of RSs on the cell membrane permeability, β-D-galactosidase activity assay was employed accordingly. Active β-D-galactosidase can catalyze the hydrolysis of o-nitrophenyl-β-D-galactopyranoside (ONPG), producing yellow o-nitrophenol

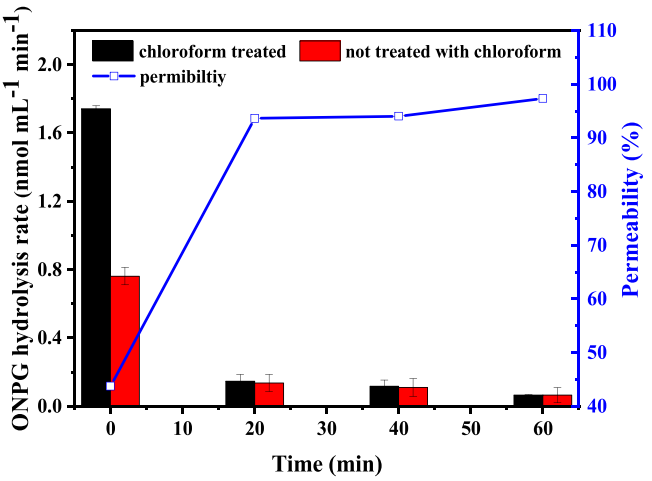

Fig. 4. β-D-Galactosidase activity and membrane permeability of the treated cells by the collaboration system.

(ONP) (Xia et al., 2015; Sun et al., 2014; Huang et al., 2000). It can be seen from the Fig. 4 that, the hydrolysis rate of ONPG dropped rapidly within the first 20 min, regardless of whether the cells were treated with chloroform (where ONPG have free access to β-D-galactosidase) or not. This strongly indicated the β-D-galactosidase was inactivated obviously by the synergistic effect from the persulfate, BiO_{2-x} and NIR irradiation composed collaboration system, coincided with the bacterial death. For the cells that have not been treated with chloroform, the ONPG hydrolysis rate at the beginning was comparatively much lower, as the diffusion ability of ONPG across the intact cell membrane is limited by the barrier posed by the cell membrane and the availability of lactose permease. The variance of these two hydrolysis rates revealed the membrane permeability changes of the cells treated by the persulfate, BiO_{2-x} and NIR irradiation composed collaboration system. And as shown in Fig. 4, the membrane permeability increased significantly after 20 min treatment, further suggesting the impaired membrane structure.

When proteins were oxidatively attacked, the side-chain amine groups on several amino acids (i.e., lysine, arginine, proline or histidine) of proteins can be transformed into carbonyls (Xiao et al., 2020). Protein carbonyl (PC) is the most general and commonly used indicator of the oxidation injury to the protein (Stadtman, 1990). The increase of PC content during the first 40 min of irradiation time (Fig. 3c), suggesting that the generated RSs (h^+, sulfate radicals, H_2O_2, O_2^- etc.) induced severe oxidation injury to protein. And for the decrease of PC after 40 min, it may be ascribed to the further oxidation or mineralization of the carbonylated protein by the sulfate radical.

However, oxidative damages might not be completely lethal to the bacteria cells, as self-repair and regrowth would take place under the right conditions. Only severe damage or loss of the genetic materials is lethal to the cells (Zhang et al., 2015). As seen in Fig. 3d, after treated by the collaborating system, both the leakage of DNA and RNA increased apparently, implying the complete impairment of the genetic system and the lethal damage to the bacteria cells by RSs during the disinfection process. And the observed decrease of DNA leakage after 20 min of treatments is highly possibly ascribed to the further disintegration caused by the RSs.

In addition, the membrane destruction was more directly observed by fluorescent staining (Fig. 3e) and SEM observation (Fig. 3f). When stained by the penetrative green-fluorescent nucleic acid stain (SYTO 9) and the non-penetrative red-fluorescent stain (propidium iodide, PI), the live bacteria cells with intact membrane would emit green fluorescence, whereas those dead cells with incomplete membrane would emit red fluorescence. Before the irradiation, the initial untreated bacteria presented intense green fluorescence. After 30 min of treatment, increasing emission of red fluorescence was observed, suggesting a gradual loss of

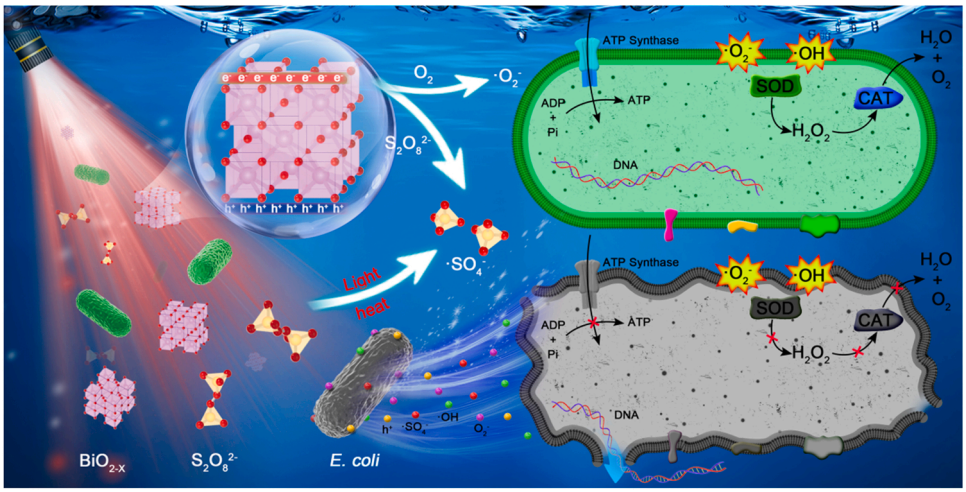

Scheme 1. Proposed bacterial inactivation mechanism of the collaborating system under NIR irradiation.

the cell membrane integrity. The emitted intensive red fluorescence at 60 min solidly demonstrated the disintegration of cell membranes. As shown in Fig. 3f, the great contrast between the well-preserved smooth surface (without treatment) and the rough, pitted, porous and collapsed morphology (treated) more intuitively proved the severe damages to the cells caused by the NIR irradiation, BiO_{2-x} and persulfate collaborated system.

4. Conclusions

Based on the above results, a possible mechanism toward the distinctive collaborating system was proposed (Scheme 1). The NIR responsive BiO_{2-x} nanoplates and persulfate formed a strong synergy effect under NIR irradiation. On one hand, the NIR irradiation induced direct light/heat activation mode of persulfate can be further enhanced by the involvement of BiO_{2-x} owing to its impressive light absorption ability. On the other hand, the NIR irradiation could photocatalytically activate BiO_{2-x} to generate active holes and electrons. The e^- cannot only reduce persulfate to produce sulfate radical, but also can react with O_2 to form O_2^-. Therefore, the activation of persulfate in the collaboration system is multi-channel, guaranteeing the sufficient effects of sulfate radicals on the *E. coli* disinfection. Then SO_4^- work collaboratively with other reactive species (O_2^-, h^+ and ·OH) to sterilize the bacterial cells. After being attacked, the cell membrane and membrane-associated functions were gradually being destroyed, evidenced by the conformational change of the membrane and dramatic loss of the respiration activity and ATP synthesis capacity. This was followed by the intense oxidation of cytoplasmic proteins and lipids. Finally, DNA and RNA were leaked out, causing the complete and irreversible death of bacteria cells.

CRediT authorship contribution statement

Hongli Sun: Methodology, Data curation, Formal analysis, Writing – original draft, Funding acquisition. **Kemeng Xiao:** Methodology, Formal analysis, Writing – review & editing. **Yunfei Ma:** Data curation, Formal analysis. **Shuning Xiao:** Data curation, Formal analysis. **Qitao Zhang:** Conceptualization, Supervision, Validation, Funding acquisition, Writing – review & editing. **Chenliang Su:** Conceptualization, Supervision, Validation, Funding acquisition, Writing – review & editing. **Po Keung Wong:** Conceptualization, Supervision, Validation, Writing – review & editing.

Declaration of Competing Interest

The authors declare that they have no known competing financial interests or personal relationships that could have appeared to influence the work reported in this paper.

Acknowledgment

The authors acknowledge the financial support of the National Natural Science Foundation of China (Nos. 22102102, 21805191 and 21972094), China Postdoctoral Science Foundation (2021T140472), the Guangdong Basic and Applied Basic Research Foundation (No. 2020A1515010982), Shenzhen Pengcheng Scholar Program, Shenzhen Peacock Plan (No. KQTD20160531120429 71), Shenzhen Science and Technology Program (Nos. KQJSCX20170727100802505 and RCJC20200714114434086), Shenzhen Stable Support Project (20200812122947002) and Graduate Innovation and Development Fund Project of Shenzhen University (315-0000470620). The authors also thank Dr. Nan Jian from the Electron Microscope Center of the Shenzhen University for his help in HRTEM measurement.

Appendix A. Supporting information

Supplementary data associated with this article can be found in the online version at doi:10.1016/j.jhazmat.2022.128510.

References

Ahmad, M., Teel, A.L., Watts, R.J., 2013. Mechanism of persulfate activation by phenols. Environ. Sci. Technol. 47, 5864–5871.
An, T.C., Zhao, H.J., Wong, P.K., 2016. Advances in Photocatalytic Disinfection. Springer-Verlag GmbH Germany.
Anipsitakis, G.P., Dionysiou, D.D., 2003. Degradation of organic contaminants in water with sulfate radicals generated by the conjunction of peroxymonosulfate with cobalt. Environ. Sci. Technol. 37, 4790–4797.
Antoniou, M.G., Cruz, A.A., Dionysiou, D.D., 2010. Degradation of microcystin-LR using sulfate radicals generated through photolysis, thermolysis and e− transfer mechanisms. Appl. Catal. B Environ. 96, 290–298.
Bangun, J., 1998. The photodegradation kinetics of aqueous sodium oxalate solution using TiO_2 catalyst. Appl. Catal. A Gen. 175, 221–235.
Bao, J., Zhang, X., Fan, B., Zhang, J., Zhou, M., Yang, W., Hu, X., Wang, H., Pan, B., Xie, Y., 2015. Ultrathin spinel-structured nanosheets rich in oxygen deficiencies for enhanced electrocatalytic water oxidation. Angew. Chem. Int. Ed. Engl. 54, 7399–7404.
Catala, A., Diaz, M., 2016. Editorial: impact of lipid peroxidation on the physiology and pathophysiology of cell membranes. Front. Physiol. 7, 423.
Chen, Y., Lu, A., Li, Y., Zhang, L., Yip, H.Y., Zhao, H., An, T., Wong, P.K., 2011. Naturally occurring sphalerite as a novel cost-effective photocatalyst for bacterial disinfection under visible light. Environ. Sci. Technol. 45, 5689–5695.
Gaschler, M.M., Stockwell, B.R., 2017. Lipid peroxidation in cell death. Biochem. Biophys. Res. Commun. 482, 419–425.

Gorle, G., Bathinapatla, A., Chen, Y.-Z., Ling, Y.-C., 2018. Near infrared light activatable PEI-wrapped bismuth selenide nanocomposites for photothermal/photodynamic therapy induced bacterial inactivation and dye degradation. RSC Adv. 8, 19827–19834.

Gu, X., Lu, S., Li, L., Qiu, Z., Sui, Q., Lin, K., Luo, Q., 2011. Oxidation of 1,1,1-trichloroethane stimulated by thermally activated persulfate. Ind. Eng. Chem. Res. 50, 11029–11036.

Huang, H., Zhou, C., Jiao, X., Yuan, H., Zhao, J., He, C., Hofkens, J., Roeffaers, M.B.J., Long, J., Steele, J.A., 2020. Subsurface defect engineering in single-unit-cell Bi_2WO_6 monolayers boosts solar-driven photocatalytic performance. ACS Catal. 10, 1439–1443.

Huang, Z., Maness, P.-C., Blake, D.M., Wolfrum, E.J., Smolinski, S.L., Jacoby, W.A., 2000. Bactericidal mode of titanium dioxide photocatalysis. J. Photochem. Photobiol. A 130, 163–170.

Huie, R.E., Clifton, C.L., 1996. Kinetics of the reaction of the sulfate radical with the oxalate anion. Int. J. Chem. Kinet. 28, 195–199.

Keane, D.A., McGuigan, K.G., Ibáñez, P.F., Polo-López, M.I., Byrne, J.A., Dunlop, P.S.M., O'Shea, K., Dionysiou, D.D., Pillai, S.C., 2014. Solar photocatalysis for water disinfection: materials and reactor design. Catal. Sci. Technol. 4, 1211–1226.

Khan, S., He, X., Khan, J.A., Khan, H.M., Boccelli, D.L., Dionysiou, D.D., 2017. Kinetics and mechanism of sulfate radical- and hydroxyl radical-induced degradation of highly chlorinated pesticide lindane in UV/peroxymonosulfate system. Chem. Eng. J. 318, 135–142.

Kochany, J., Kochany, E.L., 1992. Application of the EPR spin - trapping technique for the investigation of the reactions of carbonate, bicarbonate, and phosphate anions with hydroxyl radicals generated by the photolysis of H_2O_2. Chemosphere 25, 1769–1782.

Lau, T.K., Chu, W., Graham, N.J.D., 2007. The aqueous degradation of butylated hydroxyanisole by UV/$S_2O_8^{2-}$: study of reaction mechanisms via dimerization and mineralization. Environ. Sci. Technol. 41, 613–619.

Lee, J., von Gunten, U., Kim, J.H., 2020. Persulfate-based advanced oxidation: critical assessment of opportunities and roadblocks. Environ. Sci. Technol. 54, 3064–3081.

Li, B., Tan, L., Liu, X.M., Li, Z.Y., Cui, Z.D., Liang, Y.Q., Zhu, S.L., Yang, X.J., Yeung, K.W. K., Wu, S.L., 2019. Superimposed surface plasma resonance effect enhanced the near-infrared photocatalytic activity of Au@Bi_2WO_6 coating for rapid bacterial killing. J. Hazard. Mater. 380.

Li, H., Shi, J., Zhao, K., Zhang, L., 2014. Sustainable molecular oxygen activation with oxygen vacancies on the {001} facets of BiOCl nanosheets under solar light. Nanoscale 6, 14168–14173.

Li, H., Qin, F., Yang, Z., Cui, X., Wang, J., Zhang, L., 2017. New reaction pathway induced by plasmon for selective benzyl alcohol oxidation on BiOCl possessing oxygen vacancies. J. Am. Chem. Soc. 139, 3513–3521.

Li, H.T., Liu, R.H., Liu, Y., Huang, H., Yu, H., Ming, H., Lian, S.Y., Lee, S.T., Kang, Z.H., 2012. Carbon quantum dots/Cu_2O composites with protruding nanostructures and their highly efficient (near) infrared photocatalytic behavior. J. Mater. Chem. 22, 17470–17475.

Li, J., Wu, X.Y., Pan, W.F., Zhang, G.K., Chen, H., 2018. Vacancy-rich monolayer BiO_{2-x} as a highly efficient UV, visible, and near-infrared responsive photocatalyst. Angew. Chem. Int. Ed. 57, 491–495.

Li, J., Li, Y., Zhang, G., Huang, H., Wu, X., 2019. One-dimensional/two-dimensional core-shell-structured Bi_2O_4/BiO_{2-x} heterojunction for highly efficient broad spectrum light-driven photocatalysis: faster interfacial charge transfer and enhanced molecular oxygen activation mechanism. ACS Appl. Mater. Interfaces 11, 7112–7122.

Lin, Y., Han, D., Li, Y., Tan, L., Liu, X., Cui, Z., Yang, X., Li, Z., Liang, Y., Zhu, S., Wu, S., 2019. Ag_2S@WS_2 heterostructure for rapid bacteria-killing using near-infrared light. ACS Sustain. Chem. Eng. 7, 14982–14990.

Lutze, H.V., Bircher, S., Rapp, I., Kerlin, N., Bakkour, R., Geisler, M., von Sonntag, C., Schmidt, T.C., 2015. Degradation of chlorotriazine pesticides by sulfate radicals and the influence of organic matter. Environ. Sci. Technol. 49, 1673–1680.

Maness, P.C., Smolinski, S., Blake, D.M., Huang, Z., Wolfrum, E.J., Jacoby, W.A., 1999. Bactericidal activity of photocatalytic TiO_2 reaction: toward an understanding of its killing mechanism. Appl. Environ. Microbiol. 65, 4094–4098.

Qin, W.P., Zhang, D.S., Zhao, D., Wang, L.L., Zheng, K.Z., 2010. Near-infrared photocatalysis based on YF_3:Yb^{3+}, Tm^{3+}/TiO_2 core/shell nanoparticles. Chem. Commun. 46, 2304–2306.

Sang, Y.H., Zhao, Z.H., Zhao, M.W., Hao, P., Leng, Y.H., Liu, H., 2015. From UV to near-infrared, WS_2 nanosheet: a novel photocatalyst for full solar light spectrum photodegradation. Adv. Mater. 27, 363–369.

Stadtman, E.R., 1990. Metal ion-catalyzed oxidation of proteins: biochemical mechanism and biological consequences. Free Radic. Biol. Med. 9, 315–325.

Sun, H., Li, G., Nie, X., Shi, H., Wong, P.K., Zhao, H., An, T., 2014. Systematic approach to in-depth understanding of photoelectrocatalytic bacterial inactivation mechanisms by tracking the decomposed building blocks. Environ. Sci. Technol. 48, 9412–9419.

Sun, H., Yip, H.Y., Jiang, Z., Ye, L., Lo, I.M.C., Wong, P.K., 2018. Facile synthesis of oxygen defective yolk–shell BiO_{2-x} for visible-light-driven photocatalytic inactivation of Escherichia coli. J. Mater. Chem. A 6, 4997–5005.

Sun, H., Jiang, Z., Wu, D., Ye, L., Wang, T., Wang, B., An, T., Wong, P.K., 2019. Defect-type-dependent near-infrared-driven photocatalytic bacterial inactivation by defective Bi_2S_3 nanorods. ChemSusChem 12, 890–897.

Sun, H., Wang, J., Jiang, Y., Shen, W., Jia, F., Wang, S., Liao, X., Zhang, L., 2019. Rapid aerobic inactivation and facile removal of *Escherichia coli* with amorphous zero-valent iron microspheres: indispensable roles of reactive oxygen species and iron corrosion products. Environ. Sci. Technol. 53, 3707–3717.

Tan, C., Gao, N., Deng, Y., An, N., Deng, J., 2012. Heat-activated persulfate oxidation of diuron in water. Chem. Eng. J. 203, 294–300.

Tian, J., Sang, Y.H., Yu, G.W., Jiang, H.D., Mu, X.N., Liu, H., Bi2WO6-based, A., 2013. hybrid photocatalyst with broad spectrum photocatalytic properties under UV, visible, and near-infrared irradiation. Adv. Mater. 25, 5075–5080.

Wang, B., Jiang, Z., Yu, J.C., 2019. Treated rape pollen: a metal-free visible-light-driven photocatalyst from nature for efficient water disinfection. J. Mater. Chem. A 7, 9335–9344.

Wang, W., Wang, H., Li, G., An, T., Zhao, H., Wong, P.K., 2019. Catalyst-free activation of persulfate by visible light for water disinfection: efficiency and mechanisms. Water Res. 157, 106–118.

Wang, W., Wang, H., Li, G., Wong, P.K., An, T., 2020. Visible light activation of persulfate by magnetic hydrochar for bacterial inactivation: efficiency, recyclability and mechanisms. Water Res. 176, 115746.

Wu, D., An, T.C., Li, G.Y., Wang, W., Cai, Y.C., Yip, H.Y., Zhao, H.J., Wong, P.K., 2015. Mechanistic study of the visible-light-driven photocatalytic inactivation of bacteria by graphene oxide-zinc oxide composite. Appl. Surf. Sci. 358, 137–145.

Wu, D., Wang, B., Wang, W., An, T.C., Li, G.Y., Ng, T.W., Yip, H.Y., Xiong, C.M., Lee, H. K., Wong, P.K., 2015. Visible-light-driven BiOBr nanosheets for highly facet-dependent photocatalytic inactivation of *Escherichia coli*. J. Mater. Chem. A 3, 15148–15155.

Xia, D.H., Shen, Z.R., Huang, G.C., Wang, W.J., Yu, J.C., Wong, P.K., 2015. Red Phosphorus: an earth-abundant elemental photocatalyst for "green" bacterial inactivation under visible light. Environ. Sci. Technol. 49, 6264–6273.

Xia, D.H., Li, Y., Huang, G.C., Fong, C.C., An, T.C., Li, G.Y., Yip, H.Y., Zhao, H.J., Lu, A. H., Wong, P.K., 2015. Visible-light-driven inactivation of *Escherichia coli* K-12 over thermal treated natural pyrrhotite. Appl. Catal. B Environ. 176, 749–756.

Xia, D.H., Liu, H.D., Jiang, Z.F., Ng, T.W., Lai, W.S., An, T.C., Wang, W.J., Wong, P.K., 2018. Visible-light-driven photocatalytic inactivation of *Escherichia coli* K-12 over thermal treated natural magnetic sphalerite: band structure analysis and toxicity evaluation. Appl. Catal. B Environ. 224, 541–552.

Xiao, K., Wang, T., Sun, M., Hanif, A., Gu, Q., Tian, B., Jiang, Z., Wang, B., Sun, H., Shang, J., Wong, P.K., 2020. Photocatalytic bacterial inactivation by a rape pollen-MoS_2 biohybrid catalyst: synergetic effects and inactivation mechanisms. Environ. Sci. Technol. 54, 537–549.

Xu, J., Liu, N., Wu, D., Gao, Z., Song, Y.Y., Schmuki, P., 2020. Upconversion nanoparticle-assisted payload delivery from TiO_2 under near-infrared light irradiation for bacterial inactivation. ACS Nano 14, 337–346.

Yang, J., Hu, S., Fang, Y., Hoang, S., Li, L., Yang, W., Liang, Z., Wu, J., Hu, J., Xiao, W., Pan, C., Luo, Z., Ding, J., Zhang, L., Guo, Y., 2019. Oxygen vacancy promoted O_2 activation over perovskite oxide for low-temperature CO oxidation. ACS Catal. 9, 9751–9763.

Yu, Z., Rabiee, H., Guo, J., 2021. Synergistic effect of sulfidated nano zerovalent iron and persulfate on inactivating antibiotic resistant bacteria and antibiotic resistance genes. Water Res. 198, 117141.

Zhang, Q., Liu, X., Tan, L., Cui, Z., Li, Z., Liang, Y., Zhu, S., Yeung, K.W.K., Zheng, Y., Wu, S., 2020. An UV to NIR-driven platform based on red phosphorus/graphene oxide film for rapid microbial inactivation. Chem. Eng. J. 383.

Zhang, S., Ye, C., Lin, H., Lv, L., Yu, X., 2015. UV disinfection induces a VBNC state in *Escherichia coli* and *Pseudomonas aeruginosa*. Environ. Sci. Technol. 49, 1721–1728.

Zhang, X., Liu, M., Kang, Z., Wang, B., Wang, B., Jiang, F., Wang, X., Yang, D.-P., Luque, R., 2020. NIR-triggered photocatalytic/photothermal/photodynamic water remediation using eggshell-derived $CaCO_3$/CuS nanocomposites. Chem. Eng. J. 388.

Zhang, Y., Wang, L., Ma, X., Ren, J., Sun, Q., Shi, Y., Li, L., Shi, J., 2018. Up-conversion nanoparticles sensitized inverse opal photonic crystals enable efficient water purification under NIR irradiation. Appl. Surf. Sci. 435, 799–808.